



Synthesis and biological activity of selenopsammaplin A and its analogues as antitumor agents with DOT1L inhibitory activity

Hae Ju Han^{a,1}, Woong Sub Byun^{b,1}, Gyu Ho Lee^a, Won Kyung Kim^b, Kyungkuk Jang^a,
 Sehun Yang^a, Jewon Yang^a, Min Woo Ha^{c,d}, Suckchang Hong^a, Jeeyeon Lee^a, Jongheon Shin^b,
 Ki Bong Oh^e, Sang Kook Lee^{b,*}, Hyeung-geun Park^{a,*}

^a Research Institute of Pharmaceutical Science and College of Pharmacy, Seoul National University, Seoul 151-742, Republic of Korea

^b Natural Products Research Institute, College of Pharmacy, Seoul National University, Seoul 151-742, Republic of Korea

^c College of Pharmacy, Jeju National University, 102 Jejudaehak-ro, Jeju 63243, Republic of Korea

^d Interdisciplinary Graduate Program in Advanced Convergence Technology & Science, Jeju National University, 102 Jejudaehak-ro, Jeju, 63243, Republic of Korea

^e Department of Agricultural Biotechnology, College of Agriculture and Life Sciences, Seoul National University, Seoul 151-921, Republic of Korea

ARTICLE INFO

Keywords:

Selenopsammaplin A
 Structure-activity relationship
 Cytotoxicity
 DOT1L histone H3 methyltransferase
 Antimetastasis

ABSTRACT

Disruptor of telomeric silencing-1 like (DOT1L) is a histone H3 methyltransferase which specifically catalyzes the methylation of histone H3 lysine-79 residue. Recent findings demonstrate that DOT1L is abnormally overexpressed and the upregulated DOT1L evokes the proliferation and metastasis in human breast cancer cells. Therefore, the DOT1L inhibitor is considered a promising strategy to treat breast cancers. Non-nucleoside DOT1L inhibitors, selenopsammaplin A and its analogues, were firstly reported in the present study. Selenopsammaplin A was newly designed and synthesized with 25% overall yield in 8 steps from 3-bromo-4-hydroxybenzaldehyde, and thirteen analogues of selenopsammaplin A were prepared for structure-activity relationship studies of their cytotoxicity against cancer cells and inhibitory activity toward DOT1L for antitumor potential. All synthetic selenopsammaplin A analogues exhibited the higher cytotoxicity compared to psammaplin A with up to 6–60 times depending on cancer cells, and most analogues showed significant inhibitory activities against DOT1L. Among the prepared analogues, the phenyl analogue (**10**) possessed the most potent activity with both cytotoxicity and inhibition of DOT1L. Compound **10** also exhibited the antitumor and antimetastatic activity in an orthotopic mouse metastasis model implanted with MDA-MB-231 human breast cancer cells. These biological findings suggest that analogue **10** is a promising candidate for development as a cancer chemotherapeutic agent in breast cancers.

1. Introduction

The overall survival rate of cancer patients is affected not only by the use of appropriate anticancer drugs but also by the inhibition of cancer cell metastasis. Disruptor of telomeric silencing-1 like (DOT1L), a histone H3 methyltransferase, specifically catalyzes the methylation of histone H3 on the lysine-79 residue (H3K79). DOT1L-mediated H3K79 methylation is considered to be strongly associated with various biological processes, such as embryonic cell development, cell division

checkpoint, and the DNA stability.^{1,2} Recent findings also suggested that the overexpression of DOT1L and hyperactivation of DOT1L-mediated H3K79 methylation may play a crucial role in the initiation and maintenance of mixed lineage leukemia (MLL)-rearranged leukemia. Therefore, DOT1L is considered a promising therapeutic target in the development of anticancer agents for MLL-rearranged leukemia.^{3–5} In addition, recent evidence has also suggested that DOT1L may solely function as an oncogene in solid tumors including breast cancer without MLL fusion.^{6–8} In particular, DOT1L transactivates epithelial-

Abbreviations: DNMT, DNA methyltransferase; FBS, Fetal bovine serum; HDAC, Histone deacetylase; IC₅₀, Half maximal inhibitory concentration; HRP, Horseradish Peroxidase; PsA, Psammaplin A; PVDF, polyvinylidene fluoride; SDS, sodium dodecyl sulfate; SRB, Sulforhodamine B; TBS, Tris-buffered saline; TCA, trichloroacetic acid; EMT, epithelial-mesenchymal transition; PAGE, polyacrylamide gel electrophoresis; H&E, hematoxylin and eosin.

* Corresponding authors.

E-mail addresses: hansy0574@snu.ac.kr (H. Ju Han), sky_magic@naver.com (W. Sub Byun), sklee61@snu.ac.kr (S. Kook Lee), hgpk@snu.ac.kr (H.-g. Park).

¹ Co-first author

<https://doi.org/10.1016/j.bmc.2021.116072>

Received 19 January 2021; Received in revised form 3 February 2021; Accepted 4 February 2021

Available online 11 February 2021

0968-0896/© 2021 Elsevier Ltd. All rights reserved.

mesenchymal transition (EMT)-promoting genes, which is an essential process for cancer cell invasion and metastasis⁹, suggesting that DOT1L is a suitable molecular target for the development of antitumor and antimetastasis therapeutics for aggressive breast cancer. Since the DOT1L histone H3 methyltransferase has been recognized as a promising target for the development of novel anticancer agents, efforts to identify effective DOT1L inhibitors have also become common.^{10,11} To date, however, only a few nucleoside-type inhibitors have been reported and no other classes of small molecules have been developed.¹² (see Fig 1.).

As part of our ongoing search for novel antimetastatic cancer chemotherapeutic agents targeting histone-modifying enzymes, we recently developed very efficient synthetic methods for preparing psammaplin A and its analogues, and evaluated their cytotoxicity.¹⁴ However, only a few compounds have exhibited antitumor activity comparable to psammaplin A itself in both in vitro cell culture and in vivo xenograft mouse models and poor antimetastatic activity (see Fig 2).

Selenium, the element with atomic number 34, belongs to the same family as oxygen and sulfur in the periodic table. It is a trace element present in the body as part of 21st amino acid, selenocysteine (SeC), but it is essential for metabolism, and has been shown to have anticancer effects.²⁵ As oxidative stress is known to be associated with carcinogenesis, the anticancer activity of selenium might be due to the antioxidant properties of selenium-containing proteins (selenoproteins), including proteins in the glutathione peroxidase family and selenoprotein P, which has been tested against bladder cancer, breast cancer, prostate cancer, lung cancer and colon cancer.^{26–29} Selenium involved organic compounds have also been reported to induce apoptosis of cancer cells and to exhibit anticancer effects in prostate cancer, colorectal cancer, liver cancer, and blood cancer.³⁰ In addition, as selenium has more lipophilic physicochemical properties than oxygen and sulfur, its presence in organic molecules can result in better oral bioavailability by better penetration across the cell membrane, including the blood–brain barrier (BBB). Based on these findings, seleno-acyclovir (1)³¹, seleno-adefovir³², and seleno-tenofovir (2)^{33,34} have been successfully reported as efficient anti-viral agents.

As part of our focus on the anticancer effects of organo-selenium, we designed the novel selenopsammaplin A (9) with improved anticancer activity by replacing the disulfide bond in psammaplin A with a diselenide bond. Herein, we report a new synthetic method for accessing selenopsammaplin A (9) and its analogues with a structure–activity relationship by evaluating cytotoxicity and DOT1L inhibitory activity. In addition, the in vivo antitumor activity and antimetastatic activity of a selected compound was determined by employing an orthotopic mouse metastasis models implanted with human breast cancer cells.

2. Results and discussion

2.1. Chemistry

First, the synthesis of selenopsammaplin A (9) was attempted by modifying the synthetic route (Scheme 1) to psammaplin A.¹³ We

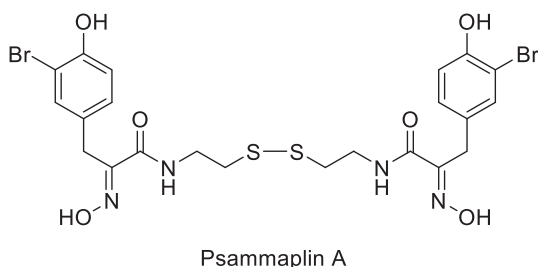


Figure 1. Structure of psammaplin A^{15–24}.

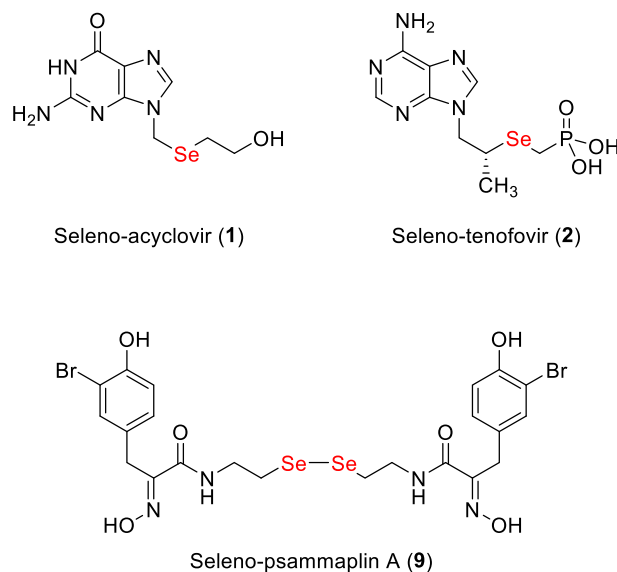


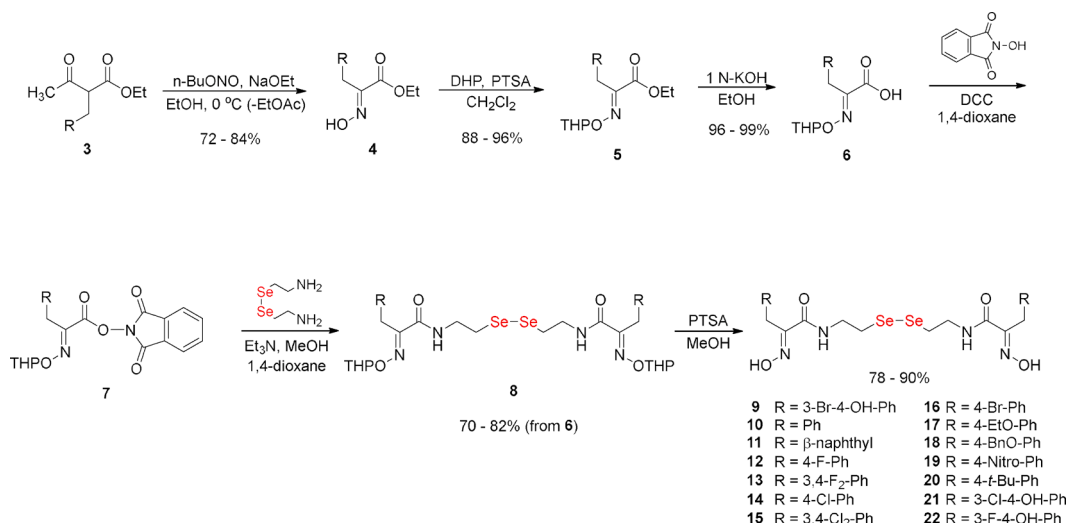
Figure 2. Structure of seleno-acyclovir (1), seleno-tenofovir (2), and selenopsammaplin A (9).

prepared compound 3 via the Knoevenagel condensation followed by reduction from ethyl acetoacetate and 3-bromo-4-hydroxybenzaldehyde according to the previous method.¹³ The direct α -nitrosation of 3 by treatment with *n*-butylnitrite in basic condition of sodium ethoxide under ethanol at 0 °C produced oxime 4 via α -NO-substitution followed by subsequent rearrangement.

Selective THP protection of 4 in the presence of catalytic amount of *p*-toluenesulfonic acid in methylene chloride at room temperature afforded 5 (95%). Then, the ethyl ester of 5 was hydrolyzed to corresponding acid 6 with 1 N KOH in ethanol (99%). Activation of 6 by coupling with *N*-hydroxyphthalimide using DCC in 1,4-dioxane afforded 7. Without purification, the addition of selenocystamine to 7 generated dimer 8. Finally, selenopsammaplin A (9) could be obtained by THP deprotection in acidic conditions (84%). Using the optimized synthetic method, thirteen analogues of selenopsammaplin A (10–22) were prepared from the corresponding aldehydes (Scheme 1). Before we performed the evaluation their biological activities, we needed to confirm the chemical stability of selenopsammaplin A and its analogues. Selenopsammaplin A (9) was dissolved in a mixture of dimethylsulfoxide and 0.1 M phosphate buffer (pH 7.0) (1:1). After 48 h at room temperature, there was no significant changes, such as cleavage of diselenide bond or hydrolysis of oxime groups.

2.2. Cytotoxic activity of selenopsammaplin A analogues and structure–activity relationship

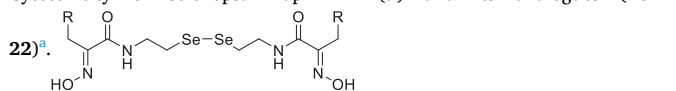
The cytotoxicity of selenopsammaplin A (9) and its analogues (10–22) were examined against a panel of human cancer cell lines. As shown in Table 1, the analogues of selenopsammaplin A showed cytotoxicity up to 6–60 times greater than that of psammaplin A itself depending on cancer cells. As a result, the size of the aromatic group affects to cytotoxicity. Larger substituents result in lower cytotoxicity (entries 2, 3, 12, 10 > 11, 20; entries 9–10, 17 > 18). In the case of halides, there was no significant difference in the cytotoxicity except for 4-fluoro analogue 12 (entries 4–8). However, the 3-fluoro-4-hydroxy analogue (entry 14, 22) and the 3-chloro-4-hydroxy analogue (entry 13, 21) afforded the best activities, and their activities were similar to that of selenopsammaplin A (9). Notably, unsubstituted analogue 10 showed a higher cytotoxicity than other substituted analogues except the 3-halide-4-hydroxy analogues (9, 21, and 22). To further confirm whether the compounds selectively suppress the cancer cells, the active compounds selenopsammaplin A (9) and analogue 10 were evaluated in MCF10A cells



Scheme 1. Synthesis of selenopsammaplin A (9) and its analogues (10 – 22) from various aldehydes.

Table 1

Cytotoxicity of selenopsammaplin A (9) and its analogues (10 –



Entry	R	A 549 ^b	HCT 116 ^c	MDA- MB231 ^d	SK- HEP- 1 ^e	SNU 638 ^f
1	3-Br-4-OH-Ph (9)	0.03	0.01	0.16	0.21	0.02
2	Ph (10)	0.08	0.09	0.06	0.12	0.05
3	β -naphthyl (11)	0.38	0.12	0.19	0.17	0.27
4	4-F-Ph (12)	0.10	0.11	0.13	0.14	0.07
5	3,4-F ₂ -Ph (13)	0.33	0.18	0.42	0.27	0.05
6	4-Cl-Ph (14)	0.25	0.28	0.33	0.33	0.22
7	3,4-Cl ₂ -Ph (15)	0.28	0.52	0.25	0.32	0.18
8	4-Br-Ph (16)	0.31	0.17	0.39	0.31	0.15
9	4-EtO-Ph (17)	0.05	0.07	0.20	0.18	0.03
10	4-BnO-Ph (18)	0.14	0.10	0.14	0.28	0.41
11	4-Nitro-Ph (19)	0.09	0.09	0.09	0.17	0.06
12	4-t-Bu-Ph (20)	0.10	0.13	0.10	0.19	0.28
13	3-Cl-4-OH-Ph (21)	0.02	0.01	0.17	0.11	0.01
14	3-F-4-OH-Ph (22)	0.02	0.01	0.19	0.13	0.02
15	Psammaplin A (PsA)	1.76	0.61	1.31	1.29	0.56
16	Etoposide	0.30	1.20	8.70	0.40	0.20

^a Results are expressed as the calculated half maximal inhibitory concentrations (IC₅₀) of test compounds (μM). All values are the means of at least three experiments.

^b Human lung cancer cells.

^c Human colon cancer cells.

^d Human breast cancer cells.

^e Human liver cancer cells.

^f Human stomach cancer cells.

(normal human breast epithelial cell line). The IC₅₀ values of compound 9 and 10 were 16.14 μM and 18.11 μM , respectively, against MCF10A cells which showed over 100-fold higher cytotoxicity against a panel of cancer cells.

2.3. Histone H3 Lysine79 methyltransferase (DOT1L) inhibitory activity of selenopsammaplin A analogues

A series of selenopsammaplin A (9) and its analogues were evaluated in the DOT1L cell-free enzyme activity assay to identify non-nucleoside small-molecule DOT1L inhibitors. Among the tested analogues, eight compounds (9, 10, and 17 – 22) including selenopsammaplin A (9) at a test concentration of 200 nM showed significant inhibitory effects on the

DOT1L enzyme activity, while psammaplin A (PsA) showed negligible inhibition against DOT1L at a tested concentration (Figure 3A).

Since selenopsammaplin A (9) and some of its analogues exhibited DOT1L inhibitory activity in cell-free biochemical assay, we further assessed the expression level of H3K79 di-methylation (H3K79me₂), the biological target of DOT1L, by Western blotting analysis in MDA-MB-231 cells. MDA-MB-231 cells are known to exhibit overexpressed H3K79me₂ due to the hyperactivation of DOT1L.^{35,36} Consistent with the data for cell-free enzyme activity, selenopsammaplin A (9) and some of its analogues (compound 10 and 17 – 22) significantly down-regulated expression level of H3K79me₂ (Figure 3B). The β -naphthyl derivative (11) did not possess inhibitory activity, indicating that a relatively larger R group decreases the DOT1L inhibitory activity. Notably, analogues with only halide substituents (12 – 16) were less active than analogues with other functional groups. The derivative with a simple phenyl substituent at the R position (10) exhibited the most potent inhibitory activity both in cell-free enzyme activity and DOT1L-mediated H3K79me₂ expression (Figure 3A and 3B). Moreover, to confirm whether the inhibition of histone lysine residue methylation by the compound 10 is selective on DOT1L-mediated H3K79 methylation, the methylation status of other histone H3 lysine residues (K4, K27, K36) were determined by Western blotting analysis. As shown in Figure 3C, compound 10 exhibits remarkably selective inhibitory effects on H3 lysine 79 residues over other histone H3 lysine residues in MDA-MB-231 cells. However, the effect of psammaplin A (PsA) on the methylation of histone H3 residues at a concentration of 200 nM was negligible (Figure 3C). These findings suggest that selenopsammaplin A analogues are considered promising non-nucleoside inhibitors of DOT1L.

2.4. Antimetastatic activity and regulation of EMT-associated biomarkers by compound 10 in human breast cancer cells

It was reported that the hypermethylation of H3K79 is highly correlated with the enhancement of breast cancer metastasis via modulation of EMT pathway.^{16,17} Therefore, the effect of 10 on metastatic activity was evaluated by employing cell migration and invasion assays in aggressive and highly metastatic MDA-MB-231 human breast cancer cells. As depicted in Figures 4A and 4B, compared to vehicle-treated control cells, compound 10 effectively suppressed wound closure (cell migration) and invasion of cancer cell through Matrigel-coated invasion chamber in a concentration-dependent manner, but psammaplin A (PsA) was not capable to inhibit the migration and invasion of cancer cells at a concentration of 400 nM. To further determine whether the mechanism of the inhibitory activity of compound 10 toward cell migration and

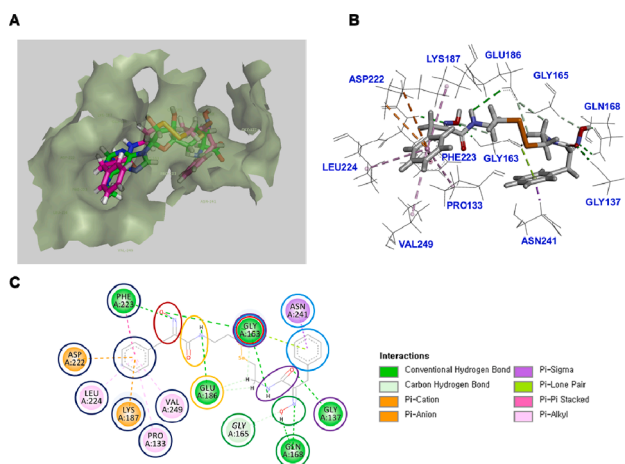


Figure 5. Predicted binding mode of **10** from the docking analysis. (A) The overlaid structures of **10** (pink) with the original ligand (TTS, green) docked into the X-ray crystal structures of the human DOT1L (PDB code: 3SR4). (B) Docked pose of **10** with the highest docking score, demonstrating hydrogen bonds (green) and hydrophobic interactions (pink). (C) Interaction diagram of **10** with the DOT1L key residues.

the ligand forms a hydrogen bond with the carboxylate side chain of Glu186. The NH of the other amide forms a hydrogen bond with the carbonyl oxygen of Gly163, whereas the carbonyl oxygen of the amide is hydrogen bonded with the NH of Gly137. The OH of the next oxime forms a hydrogen bond with the carbonyl group in the side chain of Gln168. The nearby phenyl group forms a pi-sigma hydrophobic interaction with Asn241 inside the pocket. Note that Phe223, Asp222, Glu186, Lys187, Gln168, and Gly163 are critical residues for the specific recognition between the original cofactor (SAM) and DOT1L.³⁷

2.6. Effects of compound **10** on tumor growth and metastatic potential in mouse metastasis model

The antitumor and antimetastatic activities of compound **10** were determined using an in vivo orthotopic mouse metastasis model implanted with luciferase-expressing MDA-MB-231 cells. The cells were implanted onto the fourth fat pad of the mice, and after the tumor size reached approximately 200 mm³, compound **10** (5 or 15 mg/kg), psammoplan A (PsA, 30 mg/kg), or paclitaxel (5 mg/kg) was intraperitoneally administered to each mouse thrice per week for 38 days. Compared to the control groups, compound **10** significantly inhibited tumor growth, and at the end of the experiments, the inhibition rates were 45.5% and 55.1% at 5 mg/kg and 15 mg/kg, respectively, for compound **10** (Figure 6A). The excised tumor weights measured on the termination day of the experiment were also significantly lower after treatment with compound **10** compared to those of control groups (Figure 6B). No body weight changes or overt toxicity were found in the in vivo experiments with compound **10**, while body weight loss was moderately observed in the group of paclitaxel treatment (Figure 6C). Tumor growth and incidence of metastasis were also determined by using IVIS to confirm the antitumor and antimetastatic potential of compound **10**. It was found that the luciferase signals were decreased by compound **10** treatment at the primary tumor sites (fat pad of the mouse), and the signal intensity in excised lung tissues was also effectively decreased by compound **10** treatment (Figure 6D and 6E).

Moreover, the incidence of metastatic cells in the lung was manifestly suppressed by compound **10** compared to the vehicle-treated groups (Figure 7A). These findings indicate that the primary tumor growth and lung metastasis was effectively inhibited by compound **10** in in vivo animal models. To further confirm whether the antitumor and antimetastatic activities of compound **10** are correlated with the inhibition of DOT1L-mediated H3K79 methylation and the regulation of

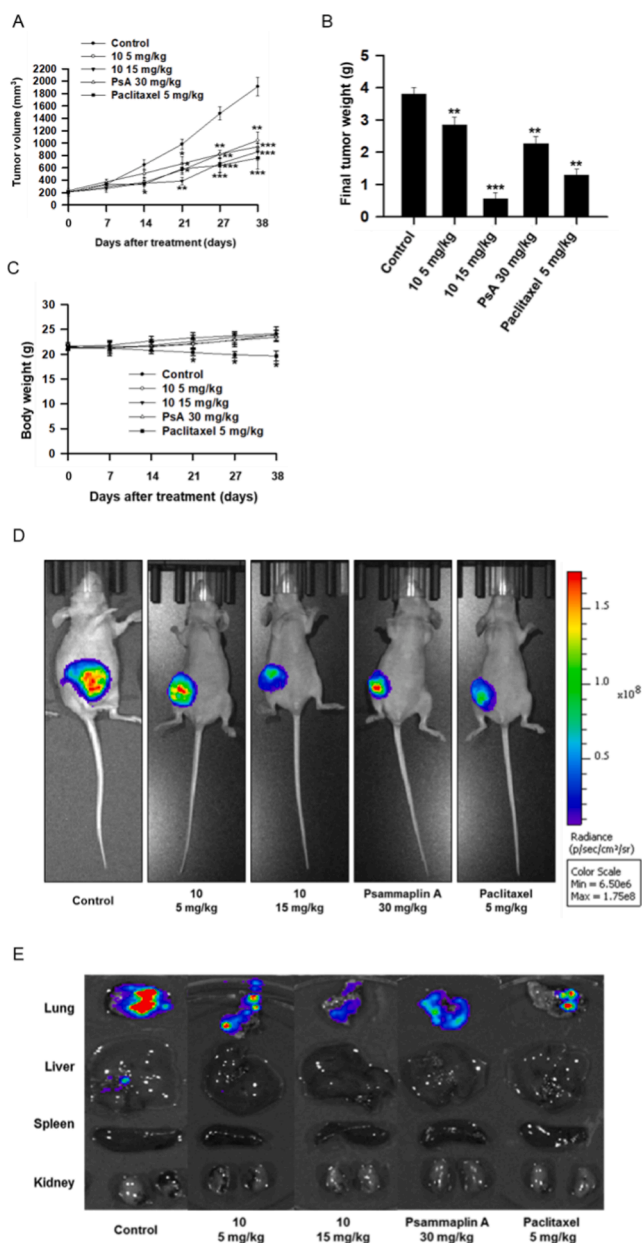


Figure 6. Antitumor and antimetastatic activities of compound **10** in an MDA-MB-231-bearing orthotopic mouse metastasis model. (A) Tumor volumes in the MDA-MB-231 orthotopic mouse metastasis model. Vehicle, compound **10**, PsA, or paclitaxel were administered thrice per week for 38 days. Tumor volumes were measured every 3 days with electronic caliper. (B) Primary tumors from mouse fat pad were excised from mice at the termination of the experiment, and tumor weights were measured. * $p < 0.05$, ** $p < 0.01$, and *** $p < 0.001$ indicate significant differences relative to the vehicle-treated control group. (C) Body weights of the mice were measured once a week. (D) Luciferase imaging (IVIS) of each group of the mice was detected on the last day of the experiment. (E) Organs (lungs, livers, spleens, and kidneys) of mice were excised from mice at the termination of experiment, and fluorescence intensity was imaged by IVIS. Control data (vehicle- and paclitaxel-treated controls) were shared with previously reported in *Mol Ther Oncolytics* 15 (2019) 140.³⁵

EMT markers, additional biochemical analyses of excised tumor tissues were performed by Western blotting. Compound **10** remarkably down-regulated the expressions of H3K79me2 and vimentin and upregulated the expression of E-cadherin in excised tumor tissues in a dose-dependent manner (Figure 7B). In addition, compound **10** also down-regulated the expression levels of Ki67, a biomarker of cell proliferation, vimentin, and H3K79me2, while compound **10** upregulated the

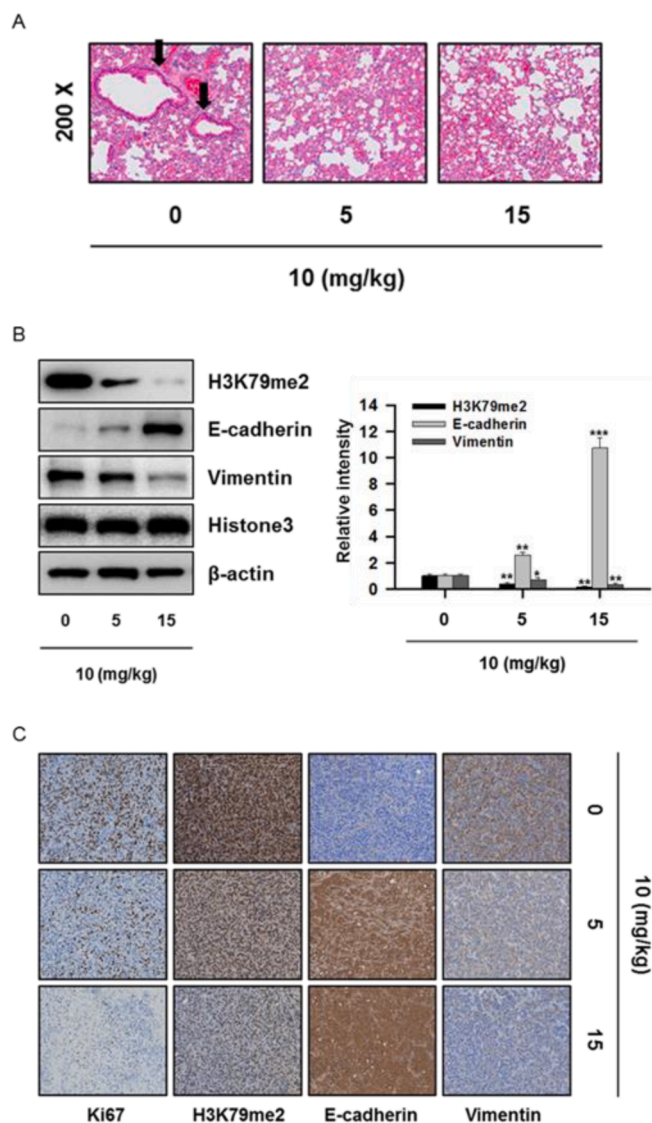


Figure 7. Compound **10** suppresses tumor growth and lung metastasis by regulating DOT1L-mediated H3K79 methylation (A) Representative hematoxylin and eosin staining of excised lungs in the orthotopically implanted mouse metastasis model; arrow, metastasized cells. (B) Small portions of tumors from each group were homogenized in complete lysis buffer (active motif). The expression levels of indicated proteins were determined by western blotting analysis using antibodies against H3K79me2, E-cadherin, and vimentin. β -Actin was used as an internal control. The relative intensity of indicated proteins was semiquantified using the NIH ImageJ software. (C) Immunohistochemical analysis was performed for the detection of Ki67, H3K79me2, E-cadherin, and Vimentin. MDA-MB-231/Luc tumor sections were counterstained with hematoxylin and imaged with Vectra 3.0 Automated Quantitative Pathology Imaging System (PerkinElmer, $200\times$). All data are representative of three separate experiments. * $p < 0.05$, ** $p < 0.01$, and *** $p < 0.001$ indicate significant differences relative to the vehicle-treated control group.

expression of E-cadherin (Figure 7C). These findings suggest that the antitumor and antimetastatic activities of compound **10** in breast cancer cells might be associated in part with the regulation of DOT1L-mediated H3K79 methylation and the EMT processes.

3. Conclusion

The present study reports that we designed and synthesized the novel selenopsammaplin A and its analogues by replacing the disulfide bond in psammaplin A with a diselenide bond. We prepared fourteen analogues

from the corresponding aldehydes by employing a Knoevenagel condensation, an α -nitrosation, and a dimerization with selenocystamine as the key steps. A structure–activity relationship study with the prepared selenopsammaplin A analogues was performed to evaluate their cytotoxicity in a panel of cancer cells and the inhibition of DOT1L in aggressive human breast cancer cells. All of the selenopsammaplin A analogues showed cytotoxicities greater than that of psammaplin A, and some of the analogues significantly inhibited DOT1L. Representative compound **10** exhibited an excellent cytotoxicity and ability to inhibit DOT1L in vitro. Antitumor and antimetastatic activities were also found in an in vivo mouse metastasis model involving the implantation of human breast cancer cells. The underlying molecular mechanism of the antimetastatic activity of compound **10** might be through the regulation of the EMT process by the inhibition of DOT1L-mediated H3K79 methylation. Taken together, these findings give an information that the antitumor and antimetastatic activities of novel selenopsammaplin A analogues via regulation of histone methylation in breast cancer cells, and DOT1L may be a promising target in the development of anticancer agents for metastatic breast cancers.

4. Experimental section

4.1. Chemistry

All reagents purchased from commercial sources were used without further purification. TLC analyses were performed using pre-coated TLC plate (silica gel 60 GF254, 0.25 mm). Flash column chromatography was performed on flash silica gel 230 ~ 400 mesh size. Infrared analyses (KBr pellet) were performed by FT-IR. ^1H NMR spectra was recorded at 300 MHz, 400 MHz, 500 MHz or 800 MHz with reference to CDCl_3 (δ 7.24), CD_3OD (δ 3.31), or $\text{DMSO}-d_6$ (δ 2.49). ^{13}C NMR spectra was obtained by 75 MHz, 100 MHz, 125 MHz or 200 MHz spectrometer relative to the central CDCl_3 (δ 77.0), CD_3OD (δ 49.0) or $\text{DMSO}-d_6$ (δ 39.5) resonance. Coupling constants (J) in ^1H NMR are in Hz. Low-resolution mass spectra (LRMS) and high-resolution mass spectra (HRMS) were measured on positive-ion FAB spectrometer. Melting points were measured on melting point apparatus and were uncorrected.

4.2. General procedure for the synthesis of selenopsammaplin a (9) and its analogues (10 ~ 22)

(*E*)-Ethyl 3-(3-bromo-4-hydroxyphenyl)-2-hydroxyimino)propanoate (**4**). Sodium ethoxide (313 mg, 4.6 mmol) was added to solution of **3** (630 mg, 2 mmol) in ethanol (10 mL) at 0°C . *n*-Butyl nitrite (257 μL , 2.2 mmol) was added and the mixture was stirred for 3 h at rt. After completion of the reaction, the ethanol was evaporated and the residue was diluted with ethyl acetate (200 mL), washed with 1 *N*-HCl (50 mL) and brine (50 mL) in order, dried over anhydrous MgSO_4 , filtered, and concentrated *in vacuo*. The residue was purified by column chromatography (silica gel, hexane : ethyl acetate = 6 ~ 3 : 1) to afford **4** (435 mg, 72% yield) as a white solid. m.p. = 87°C ; ^1H NMR (300 MHz, CD_3OD) δ = 7.35 (d, J = 2.01 Hz, 1H), 7.05 (dd, J_1 = 8.42 Hz, J_2 = 2.04 Hz, 1H), 6.77 (d, J = 8.25 Hz, 1H), 4.21 (q, J = 6.96 Hz, 2H), 3.80 (s, 2H), 1.25 (t, J = 7.14 Hz, 3H) ppm; ^{13}C NMR (100 MHz, CD_3OD) δ = 166.1, 154.6, 152.7, 135.2, 131.1, 131.0, 117.9, 111.3, 63.4, 30.7, 15.2 ppm; FT/IR = 3347, 1720, 1493, 1420, 1288, 1203, 1023, 858, 802, 759, 725 cm^{-1} ; HRMS (FAB) calcd for $[\text{C}_{11}\text{H}_{13}\text{BrNO}_4]^+$ 302.0028, found: 302.0035. The spectral data were identical with previous results.¹³

(*E*)-Ethyl 3-(3-bromo-4-hydroxyphenyl)-2-[(tetrahydro-2H-pyran-2-yl)oxy]imino)propanoate (**5**); *p*-Toluenesulfonic acid monohydrate (25 mg, 0.1 mmol) and 3,4-dihydro-2H-pyran (DHP, 218 mg, 2.6 mmol) were added to a solution of **4** (400 mg, 1.3 mmol) in dichloromethane (6 mL) at 0°C . The mixture was stirred at rt for 6 h. After completion of the reaction, a few drops of methanol was added to the reaction mixture and stirred for 10 min. The reaction mixture was diluted with dichloromethane (150 mL), washed with aq.- NH_4Cl (30 mL) and brine (50 mL),

dried over anhydrous MgSO₄, filtered, and concentrated *in vacuo*. The residue was purified by column chromatography (silica gel, hexane : ethyl acetate = 4 ~ 2 : 1) to afford **5** (478 mg, 94% yield) as a yellow oil. ¹H NMR (300 MHz, CD₃OD) (E/Z form) : δ 7.33 (d, *J* = 2.01 Hz, 1H), 7.00 (dd, *J* = 8.34, 2.19 Hz, 1H), 6.76 (d, *J* = 8.22 Hz, 1H), 6.64 (s, 1H), 4.15 (m, 2H), 3.76 (q, *J* = 13.56 Hz, 2H), 3.53 (m, 2H), 1.73 (br, 3H), 1.51 (br, 3H), 1.16 (t, *J* = 7.14 Hz, 3H) ppm; ¹³C NMR (100 MHz, CD₃OD): δ 163.048, 151.388, 151.246, 132.713, 129.134, 128.512, 115.922, 109.390, 101.386, 62.152, 61.757, 30.072, 28.051, 24.509, 18.639, 13.621 ppm; FT-IR (KBr) 3412, 2946, 2871, 2738, 2565, 1892, 1718, 1609, 1579, 1508, 1494, 1466, 1454, 1441, 1420, 1393, 1373, 1354, 1334, 1288, 1260, 1203, 1154, 1112, 1062, 1040, 1020, 966, 927, 901, 859, 817, 802, 756, 729, 673, 627 cm⁻¹; HRMS (FAB⁺) calcd for [C₁₆H₂₁BrNO₅]⁺ = 386.0603, found = 386.0598. The spectral data were identical with previous results.¹³

(*E*)-3-(3-bromo-4-hydroxyphenyl)-2-[[tetrahydro-2H-pyran-2-yl]oxy]imino}propanoic acid (**6**). Compound **5** (450 mg, 1.2 mmol) was added to 1 M KOH solution (3.5 mL) in ethanol. The mixture was stirred for 4 h until no more **5** was observed by TLC analysis. If the reaction was not completed, the mixture was supplemented by water (1 mL). After completion of the reaction, the reaction mixture was diluted with ethyl acetate (30 mL) and extracted with 0.2 N NaOH (15 mL × 3). The aqueous phase was acidified until pH 4 using 1 N HCl in ice-water bath. Then extracted by ethyl acetate (50 mL × 3), washed with brine, dried over anhydrous MgSO₄, filtered, and concentrated *in vacuo*. The residue **6** (413 mg, 99% yield) was obtained as a pale yellow solid. m.p. = 137 °C; ¹H NMR (300 MHz, CDCl₃) : δ 7.42 (d, *J* = 2.12 Hz, 1H), 7.12 (dd, *J* = 8.40, 2.12 Hz, 1H), 6.87 (d, *J* = 8.40 Hz, 1H), 5.45 (m, 1H), 3.83 (s, 2H), 3.60 (m, 2H), 1.85 (m, 3H), 1.63 (m, 3H), ppm; ¹³C NMR (100 MHz, CDCl₃) : δ 163.53, 151.23, 150.79, 132.80, 129.93, 128.65, 116.15, 109.94, 101.80, 62.25, 29.49, 28.00, 24.73, 18.47 ppm; FT-IR (KBr) 3343, 3018, 2949, 2874, 1916, 1818, 1728, 1606, 1580, 1506, 1494, 1454, 1421, 1373, 1319, 1287, 1259, 1207, 1185, 1111, 1070, 1035, 989, 967, 927, 899, 870, 835, 806, 755, 718, 672 cm⁻¹; HRMS (FAB⁺) calcd for [C₁₄H₁₇BrNO₅]⁺ = 358.0290, found = 358.0272. The spectral data were identical with previous results.¹³

(2*E*,2'*E*)-*N,N'*-[diselanediylbis(ethane-2,1-diyl)]bis[3-(3-bromo-4-hydroxyphenyl)-2-[[tetrahydro-2H-pyran-2-yl]oxy]imino} propanamide] (**8**). *N,N'*-Dicyclohexylcarbodiimide (364 mg, 1.9 mmol) and *N*-hydroxyphthalimide (346 mg, 2.1 mmol) were added to a solution of **6** (400 mg, 1.1 mmol) in 1,4-dioxane (5 mL). The mixture was stirred for 2 h until no more **6** was observed by TLC analysis, and diluted with ethyl acetate (50 mL). The mixture was washed with water (25 mL) and brine (25 mL) in order, dried over anhydrous MgSO₄, filtered, and concentrated *in vacuo*. Without further purification, the residue (**7**) was dissolved in 1,4-dioxane (5 mL). Selenocystamine dihydrochloride (178 mg, 0.56 mmol) was dissolved in methanol (2.5 mL) with triethylamine (311 μL, 2.23 mmol). This solution was added to the reaction mixture and stirred for 4 h. After completion of the reaction, the solvent was evaporated and the residue was diluted with ethyl acetate (100 mL), washed with water (25 mL) and brine (25 mL) in order, dried over anhydrous MgSO₄, filtered, and concentrated *in vacuo*. The residue was purified by column chromatography (silica gel, hexane : acetone = 3 : 1) to afford compound **8** (377 mg, 74% yield) as a white solid. m.p. = 144 °C; ¹H NMR (300 MHz, CD₃OD) δ 7.42 (d, *J* = 2.22 Hz, 2H), 7.07 (m, 2H), 6.77 (d, *J* = 8.43 Hz, 2H), 5.37 (m, 2H), 3.82 (q, *J* = 12.64 Hz, 4H), 3.57 (m, 8H), 3.05 (t, *J* = 6.87 Hz, 4H) ppm; ¹³C NMR (200 MHz, CD₃OD) δ 165.6, 155.7, 154.8, 135.6, 131.2, 130.8, 117.9, 111.4, 103.2, 102.1, 63.9, 63.8, 56.1, 42.3, 32.4, 30.7, 30.2, 27.3, 26.9, 21.2, 20.5 ppm; FT-IR = 3371, 1658, 1534, 1493, 1423, 1358, 1285, 1209, 1017, 983, 801, 720 m⁻¹; HRMS (FAB): *m/z* [M + H]⁺ calcd for [C₃₂H₄₁Br₂N₄O₈Se₂]⁺ 925.9543, found: 925.9547.

Synthesis of Selenopsammaplin A (**9**). *p*-Toluenesulfonic acid monohydrate (6.2 mg, 0.03 mmol) was added to a solution of **8** (150 mg, 0.2 mmol) in methanol (2 mL). The mixture was refluxed for 19 h and evaporated *in vacuo* to remove methanol. The residue was diluted with

ethyl acetate (50 mL), washed with water (10 mL × 3) and brine (10 mL) in order, dried over anhydrous MgSO₄, filtered, and concentrated *in vacuo*. The residue was purified by column chromatography (silica gel, hexane : ethyl acetate = 3 ~ 1 : 1) to afford selenopsammaplin A (**9**) (103 mg, 84% yield) as a yellow solid. m.p. = 72 °C; ¹H NMR(800 MHz, DMSO-d₆) δ 11.84 (s, 2H), 10.02 (s, 2H), 8.10 (t, *J* = 5.88 Hz, 2H), 7.29 (s, 2H), 7.01 (dd, *J* = 8.28, 1.16 Hz, 2H), 6.83 (d, *J* = 8.32 Hz, 2H), 3.45 (q, *J* = 6.61 Hz, 4H), 3.01 (t, *J* = 7.08 Hz, 4H) ppm; ¹³C NMR(200 MHz, DMSO-d₆) δ 163.1, 152.3, 151.8, 132.8, 129.1, 128.8, 116.1, 108.8, 39.8, 28.2, 27.7 ppm; FT-IR = 3368, 2925, 2853, 2378, 2310, 1712, 1657, 1530, 1492, 1423, 1362, 1280, 1205, 1044, 1007,967, 781, 763, 748, 670 cm⁻¹; HRMS (FAB): *m/z* [M + Na]⁺ calcd for [C₂₂H₂₄Br₂N₄O₆Se₂Na]⁺ = 780.8291, found = 780.8281.

(2*E*,2'*E*)-*N,N'*-[diselanediylbis(ethane-2,1-diyl)]bis[2-(hydroxyimino)-3-phenylpropanamide] (**10**). Following the general procedure of selenopsammaplin A (**9**) from benzaldehyde, **10** was obtained as a yellow solid (overall 27% yield). m.p. = 139 °C; ¹H NMR(800 MHz, CD₃OD) δ 7.24 (d, *J* = 7.68 Hz, 4H), 7.19 (t, *J* = 7.68 Hz, 4H), 7.12 (t, *J* = 7.36 Hz, 2H), 3.90 (s, 4H), 3.53 (t, *J* = 6.92 Hz, 4H), 2.99 (t, *J* = 6.92 Hz, 4H) ppm; ¹³C NMR(200 MHz, CD₃OD) δ 166.7, 154.0, 138.9, 130.9, 128.0, 41.9, 30.7, 30.1 ppm; FT-IR = 3841, 3734, 3680, 2973, 2381, 2359, 2349, 2308, 1658, 1648, 1525, 1491, 1424, 1362, 1219, 1054, 1033, 1012, 772, 671, 649 cm⁻¹; HRMS (FAB): *m/z* [M + H]⁺ calcd for [C₂₂H₂₇N₄O₄Se₂]⁺ 571.0363, found: 571.0363.

(2*E*,2'*E*)-*N,N'*-[diselanediylbis(ethane-2,1-diyl)]bis[2-(hydroxyimino)-3-(naphthalen-2-yl)propanamide] (**11**). Following the general procedure of selenopsammaplin A (**9**) from 4-β-naphthylbenzaldehyde, **11** was obtained as a yellow solid (overall 29% yield). m.p. = 164 °C; ¹H NMR (800 MHz, DMSO-d₆) δ 11.93 (s, 1H), 8.15 (t, *J* = 5.84 Hz, 1H), 7.82 (m, 2H), 7.80 (m, 4H), 7.67 (s, 2H), 7.45 (m, 4H), 7.40 (d, *J* = 8.48 Hz, 2H), 3.98 (s, 4H), 3.46 (t, *J* = 6.68 Hz, 4H), 3.01 (t, *J* = 7.08 Hz, 4H) ppm; ¹³C NMR(200 MHz, DMSO-d₆) δ 163.2, 151.7, 134.5, 133.0, 131.6, 127.7, 127.5, 127.4, 127.3, 126.8, 126.0, 125.4, 29.2, 28.2, 28.2 ppm; FT-IR = 3368, 2922, 2851, 2349, 1657, 1619, 1529, 1452, 1362, 1236, 1189, 1013, 965, 847, 776, 764, 750, 721, 645, 615 cm⁻¹; HRMS (FAB): *m/z* [M + H]⁺ calcd for [C₃₀H₃₁N₄O₄Se₂]⁺ 671.0676, found: 671.0673.

(2*E*,2'*E*)-*N,N'*-[diselanediylbis(ethane-2,1-diyl)]bis[3-(4-fluorophenyl)-2-(hydroxyimino)propanamide] (**12**). Following the general procedure of selenopsammaplin A (**9**) from 4-fluorobenzaldehyde, **12** was obtained as a yellow solid (overall 26% yield). m.p. = 147 °C; ¹H NMR(800 MHz, CD₃OD) δ 7.26 (m, 4H), 6.92 (t, *J* = 8.8 Hz, 4H), 3.87 (s, 4H), 3.54 (t, *J* = 6.96 Hz, 4H), 3.01 (t, *J* = 6.96 Hz, 4H) ppm; ¹³C NMR (200 MHz, CD₃OD) δ 166.5, 164.3, 163.1, 153.9, 134.9, 132.6, 116.6, 41.9, 30.1 ppm; FT-IR = 3842, 3735, 3272, 2924, 2348, 2310, 1706, 1648, 1621, 1526, 1508, 1424, 1357, 1281, 1219, 1091, 1046, 1010, 995, 814, 772, 741, 689 cm⁻¹; HRMS (FAB): *m/z* [M + H]⁺ calcd for [C₂₂H₂₅F₂N₄O₄Se₂]⁺ 607.0174, found: 607.0167.

(2*E*,2'*E*)-*N,N'*-[diselanediylbis(ethane-2,1-diyl)]bis[3-(3,4-difluorophenyl)-2-(hydroxyimino)propanamide] (**13**). Following the general procedure of selenopsammaplin A (**9**) from 3,4-difluorobenzaldehyde, **13** was obtained as a yellow solid (overall 20% yield). m.p. = 114 °C; ¹H NMR(800 MHz, CD₃OD) δ 7.15 (m, 2H), 7.09 (m, 2H), 7.05 (m, 2H), 3.86 (d, *J* = 5.36 Hz, 4H), 3.56 (t, *J* = 6.92 Hz, 4H), 3.02 (t, *J* = 6.96 Hz, 4H) ppm; ¹³C NMR(200 MHz, CD₃OD) δ 166.3, 153.3, 152.6, 151.5, 150.4, 136.4, 127.4, 119.8, 118.7, 41.9, 30.0 ppm; FT-IR = 3840, 3735, 3269, 2923, 2348, 2310, 1648, 1608, 1516, 1425, 1283, 1219, 1115, 1048, 1010, 994, 875, 816, 772, 713, 630 cm⁻¹; HRMS (FAB): *m/z* [M + H]⁺ calcd for [C₂₂H₂₃F₄N₄O₄Se₂]⁺ 642.9986, found: 642.9969.

(2*E*,2'*E*)-*N,N'*-[diselanediylbis(ethane-2,1-diyl)]bis[3-(4-chlorophenyl)-2-(hydroxyimino)propanamide] (**14**). Following the general procedure of selenopsammaplin A (**9**) from 4-chlorobenzaldehyde, **14** was obtained as a yellow solid (overall 23% yield). m.p. = 61 °C; ¹H NMR(800 MHz, CD₃OD) δ 7.24 (m, 8H), 3.87(s, 4H), 3.54 (t, *J* = 6.96 Hz, 4H), 3.00 (t, *J* = 6.96 Hz, 4H) ppm; ¹³C NMR(200 MHz, CD₃OD) δ 166.5, 153.6, 137.8, 133.8, 132.5, 130.1, 41.9, 30.1, 30.1 ppm; FT-IR = 3840, 3735, 3284, 2925, 2854, 2372, 2310, 1748, 1658, 1527, 1489,

1426, 1360, 1204, 1090, 1015, 968, 783, 762 cm^{-1} ; HRMS (FAB): m/z [M + H]⁺ calcd for [C₂₂H₂₅Cl₂N₄O₄Se₂]⁺ 638.9583, found: 638.9586.

(2*E*,2'*E*)-*N,N'*-[diselanediybis(ethane-2,1-diy)]bis[3-(3,4-dichlorophenyl)-2-(hydroxyimino)propanamide] (**15**). Following the general procedure of selenopsammaplin A (**9**) from 3,4-dichlorobenzaldehyde, **15** was obtained as a yellow solid (overall 17% yield). m.p. = 61 °C; ¹H NMR(800 MHz, CD₃OD) δ 7.41 (d, J = 2.00 Hz, 2H), 7.35 (d, J = 8.24 Hz, 2H), 7.19 (dd, J = 8.32, 2.00, 2H), 3.87 (s, 4H), 3.55 (t, J = 6.92 Hz, 4H), 3.02 (t, J = 6.92 Hz, 4H) ppm; ¹³C NMR(800 MHz, CD₃OD) δ 166.2, 153.0, 139.8, 133.8, 132.9, 132.1, 131.9, 131.0, 41.9, 30.1, 30.0 ppm; FT/IR = 3294, 2924, 2853, 2349, 2319, 1748, 1659, 1528, 1470, 1426, 1397, 1360, 1274, 1202, 1132, 1031, 1009, 969, 876, 817, 781, 719 cm^{-1} ; HRMS (FAB): m/z [M + H]⁺ calcd for [C₂₂H₂₃Cl₄N₄O₄Se₂]⁺ 706.8804, found: 706.8806.

(2*E*,2'*E*)-*N,N'*-[diselanediybis(ethane-2,1-diy)]bis[3-(4-bromophenyl)-2-(hydroxyimino)propanamide] (**16**). Following the general procedure of selenopsammaplin A (**9**) from 4-bromobenzaldehyde, **16** was obtained as a yellow solid (overall 16% yield). m.p. = 68 °C; ¹H NMR(800 MHz, CD₃OD) δ 7.35 (d, J = 10.8 Hz, 4H), 7.18 (d, J = 8.48 Hz, 4H), 3.86 (s, 4H), 3.54 (t, J = 6.96 Hz, 4H), 3.00 (t, J = 6.92 Hz, 4H) ppm; ¹³C NMR(200 MHz, CD₃OD) δ 166.4, 153.5, 138.3, 133.2, 132.9, 121.7, 41.9, 30.2, 30.1 ppm; FT/IR = 3284, 3054, 2925, 2854, 2310, 1657, 1527, 1486, 1427, 1403, 1357, 1292, 1208, 1138, 1098, 1071, 1011, 967, 917, 856, 800, 754 cm^{-1} ; HRMS (FAB): m/z [M + H]⁺ calcd for [C₂₂H₂₅Br₂N₄O₄Se₂]⁺ 726.8573, found: 726.8575.

(2*E*,2'*E*)-*N,N'*-[diselanediybis(ethane-2,1-diy)]bis[3-(4-ethoxyphenyl)-2-(hydroxyimino)propanamide] (**17**). Following the general procedure of selenopsammaplin A (**9**) from 4-ethoxybenzaldehyde, **17** was obtained as a yellow solid (overall 22% yield). m.p. = 146 °C; ¹H NMR(800 MHz, CD₃OD) δ 11.77 (s, 2H), 8.06 (t, J = 5.88 Hz, 2H), 7.10 (d, J = 8.64 Hz, 4H), 6.78 (m, 4H), 3.95 (q, J = 6.99 Hz, 4H), 3.72 (s, 4H), 3.44 (q, J = 6.72 Hz, 4H), 3.00 (t, J = 7.12 Hz, 4H), 1.28 (t, J = 1.28 Hz, 6H) ppm; ¹³C NMR(200 MHz, CD₃OD) δ 163.2, 156.8, 152.1, 129.8, 128.5, 114.1, 62.8, 28.2, 28.0, 14.6 ppm; FT/IR = 3388, 3280, 2923, 2320, 1649, 1621, 1528, 1509, 1477, 1427, 1288, 1250, 1182, 1114, 1050, 1010, 996, 808, 693 cm^{-1} ; HRMS (FAB): m/z [M + H]⁺ calcd for [C₂₆H₃₅N₄O₆Se₂]⁺ 659.0887, found: 659.0886.

(2*E*,2'*E*)-*N,N'*-[diselanediybis(ethane-2,1-diy)]bis[3-(4-(benzyl oxy)phenyl)-2-(hydroxyimino)propanamide] (**18**). Following the general procedure of selenopsammaplin A (**9**) from 4-benzoyloxybenzaldehyde, **18** was obtained as a yellow solid (overall 27% yield). m.p. = 163 °C; ¹H NMR(800 MHz, DMSO-*d*₆) δ 11.78 (s, 2H), 8.07 (t, J = 5.88 Hz, 2H), 7.41 (d, J = 7.20 Hz, 4H), 7.37 (t, J = 7.60 Hz, 4H), 7.31 (t, J = 7.32 Hz, 2H), 7.11 (d, J = 8.64 Hz, 4H), 6.89 (d, J = 11.36 Hz, 4H), 5.03 (s, 4H), 3.73 (s, 4H), 3.45 (q, J = 6.69 Hz, 4H), 3.00 (t, J = 7.12 Hz, 4H); ¹³C NMR(200 MHz, DMSO-*d*₆) δ 163.2, 156.7, 152.1, 137.2, 129.8, 128.9, 128.4, 127.7, 127.6, 114.6, 69.1, 28.2, 28.0 ppm; FT/IR = 3381, 3224, 3033, 2924, 2854, 1650, 1620, 1528, 1509, 1454, 1426, 1379, 1359, 1292, 1246, 1176, 1105, 1076, 1040, 1007, 795, 728, 693, 627 cm^{-1} ; HRMS (FAB): m/z [M + H]⁺ calcd for [C₃₆H₃₉N₄O₆Se₂]⁺ 783.1200, found: 783.1196.

(2*E*,2'*E*)-*N,N'*-[diselanediybis(ethane-2,1-diy)]bis[2-(hydroxy imino)-3-(4-nitrophenyl)propanamide] (**19**). Following the general procedure of selenopsammaplin A (**9**) from 4-nitrobenzaldehyde, **19** was obtained as a yellow solid (overall 22% yield). m.p. = 70 °C; ¹H NMR(800 MHz, CD₃OD) δ 8.09 (d, J = 8.72 Hz, 4H), 7.49 (d, J = 8.80 Hz, 4H), 4.02 (s, 4H), 3.55 (t, J = 6.92 Hz, 4H), 3.02 (t, J = 6.92 Hz, 4H) ppm; ¹³C NMR(200 MHz, CD₃OD) δ 166.2, 152.6, 148.7, 147.1, 132.0, 125.2, 41.9, 30.9, 30.1 ppm; FT/IR = 3383, 3058, 2925, 1656, 1604, 1517, 1429, 1345, 1234, 1205, 1108, 1038, 1014, 970, 860, 815, 788, 774, 768, 762, 710, 665 cm^{-1} ; HRMS (FAB): m/z [M + H]⁺ calcd for [C₂₂H₂₅N₆O₈Se₂]⁺ 661.0064, found: 661.0071.

(2*E*,2'*E*)-*N,N'*-[diselanediybis(ethane-2,1-diy)]bis[3-(4-(tert-butyl)phenyl)-2-(hydroxyimino)propanamide] (**20**). Following the general procedure of selenopsammaplin A (**9**) from 4-*t*-butylbenzaldehyde, **20** was obtained as a yellow solid (overall 33% yield). m.p. = 88 °C; ¹H

NMR(800 MHz, DMSO-*d*₆) δ 11.79 (s, 2H), 8.07 (t, J = 5.88 Hz, 2H), 7.25 (d, J = 8.40 Hz, 4H), 7.11 (d, J = 8.16 Hz, 4H), 3.77 (s, 4H), 3.45 (q, J = 6.69 Hz, 4H), 3.01 (t, J = 7.12 Hz, 4H) ppm; ¹³C NMR(200 MHz, DMSO-*d*₆) δ 163.2, 151.9, 148.3, 133.6, 128.4, 125.0, 39.8, 34.0, 31.1, 28.4, 28.2 ppm; FT/IR = 3285, 3056, 2962, 2867, 1910, 1659, 1627, 1529, 1460, 1428, 1362, 1268, 1213, 1140, 1109, 1010, 968, 917, 859, 835, 811, 756, 707, 666 cm^{-1} ; HRMS (FAB): m/z [M + H]⁺ calcd for [C₃₀H₄₃N₄O₄Se₂]⁺ 683.1615, found: 683.1614.

(2*E*,2'*E*)-*N,N'*-[diselanediybis(ethane-2,1-diy)]bis[3-(3-chloro-4-hydroxyphenyl)-2-(hydroxyimino)propanamide] (**21**). Following the general procedure of selenopsammaplin A (**9**) from 3-chloro-4-hydroxybenzaldehyde, **21** was obtained as a pale yellow solid (overall 25% yield). m.p. = 132 °C; ¹H NMR(800 MHz, CD₃OD) δ 7.19 (d, J = 2.16 Hz, 2H), 7.02 (dd, J = 8.32, 2.08 Hz, 2H), 6.76 (d, J = 8.32 Hz, 2H), 3.78 (s, 4H), 3.54 (t, J = 6.92 Hz, 4H), 3.01 (t, J = 6.92 Hz, 4H) ppm; ¹³C NMR(200 MHz, CD₃OD) δ 166.6, 154.0, 153.4, 132.2, 131.1, 130.5, 122.1, 118.2, 41.9, 30.1, 29.6 ppm; FT/IR = 3286, 2923, 2852, 2320, 1658, 1526, 1424, 1345, 1279, 1227, 1211, 1038, 1027, 789, 781, 770, 761, 711, 665 cm^{-1} ; HRMS (FAB): m/z [M + H]⁺ calcd for [C₂₂H₂₅Cl₂N₄O₆Se₂]⁺ 670.9482, found: 670.9482.

(2*E*,2'*E*)-*N,N'*-[diselanediybis(ethane-2,1-diy)]bis[3-(3-fluoro-4-hydroxyphenyl)-2-(hydroxyimino)propanamide] (**22**). Following the general procedure of selenopsammaplin A (**9**) from 3-fluoro-4-hydroxybenzaldehyde, **22** was obtained as a yellow solid (overall 19% yield). m.p. = 191 °C; ¹H NMR(800 MHz, CD₃OD) δ 6.95 (dd, J = 12.16, 2.00 Hz, 2H), 6.87 (dd, J = 8.20, 1.28 Hz, 2H), 6.75 (t, J = 8.72 Hz, 2H), 3.79 (s, 4H), 3.55 (t, J = 6.96 Hz, 4H), 3.01 (t, J = 6.96 Hz, 4H) ppm; ¹³C NMR(200 MHz, CD₃OD) δ 166.6, 154.0, 152.8, 145.2, 130.6, 126.9, 119.2, 118.4, 41.9, 30.1, 29.7 ppm; FT/IR = 3757, 3317, 2320, 1658, 1517, 1440, 1360, 1288, 1236, 1198, 1109, 1038, 1002, 970, 880, 800, 781, 773, 702, 666 cm^{-1} ; HRMS (FAB): m/z [M + H]⁺ calcd for [C₂₂H₂₅F₂N₄O₆Se₂]⁺ 639.0073, found: 639.0074.

4.3. Cell culture

Human cancer cells (A549, HCT116, MDA-MB-231, SK-HEP-1, and SNU-638) and human breast epithelial cells (MCF10A) were obtained from the American Type Culture Collection (Manassas, VA, USA) or Korean Cell Line Bank (Seoul, Korea). The cells were cultured in an appropriate medium (Dulbecco's modified Eagle's medium for MDA-MB-231 and SK-HEP-1; Roswell Park Memorial Institute 1640 for A549, HCT116 and SNU-638 cells; Dulbecco's modified Eagle's medium: Nutrient Mixture F-12 for MCF-10A) supplemented with antibiotics-antimycotics (PSF: 100 units/mL sodium penicillin G, 100 $\mu\text{g}/\text{mL}$ streptomycin, and 250 ng/mL amphotericin B) and 10% fetal bovine serum (FBS) in an incubator containing 5% CO₂ at 37 °C. All reagents were purchased from Gibco® Invitrogen Corp. (Grand Island, NY, USA).

4.4. Cell proliferation assay

Cell proliferation was measured by Sulforhodamine B (SRB) assay.³⁸ Briefly, cells were seeded in 96-well plates and incubated for 30 min (for zero day controls) or treated with test compounds for the indicated times. After incubation, cells were fixed, dried and stained with 0.4% SRB in 1% acetic acid solution. Unbound dye was washed off and stained cells were dissolved in 10 mM Tris (pH 10.0). Absorbance was measured at 515 nm, and cell proliferation was determined. IC₅₀ values were calculated by non-linear regression analysis using TableCurve 2D v5.01 software (Systant Software Inc., Richmond, CA, USA). All reagents were purchased from Sigma-Aldrich.

4.5. DOT1L enzyme activity assay

DOT1L enzyme activity was measured using S-adenosyl methionine (SAM) as the methyl group donor and synthesized DOT1L as the

substrate (BPS Bioscience, Cat. No. 52202; San Diego, CA, USA) according to the manufacturer's instructions.

4.6. Western blotting analysis

Total cell lysates were prepared in 2 × sample loading buffer [250 mM Tris-HCl (pH 6.8), 10% glycerol, 4% sodium dodecyl sulfate (SDS), 2% β-mercaptoethanol, 0.006% bromophenol blue, 5 mM sodium orthovanadate, and 50 mM sodium fluoride, Bio-Rad]. The protein concentrations of samples were measured using the bicinchoninic acid method.³⁹ Equal amounts of protein (5–20 μg) were separated by 8–15% SDS-polyacrylamide gel electrophoresis (PAGE) and were transferred to polyvinylidene fluoride membranes (Millipore, Bedford, MA, USA). The membranes were blocked with 5% bovine serum albumin (BSA, Sigma-Aldrich) and were then probed with anti-E-cadherin, anti-N-cadherin (BD Bioscience), anti-H3K4me2, anti-H3K27me2, anti-H3K36me2, anti-H3K79me2, anti-Histone H3 (Cell Signaling Technology, Beverly, MA, USA) or anti-ZEB1, anti-Vimentin, anti-β-actin (Santa Cruz Biotechnology, Dallas, TX, USA) antibodies. The blots were detected with an enhanced chemiluminescence (ECL) detection kit (GE Healthcare, Little Chalfont, UK).⁴⁰

4.7. Wound healing assay

MDA-MB-231 cells were grown to 80–90% confluence in a 6-well plate. A confluent monolayer of the cells was artificially wounded with a 200 μL pipette tip, and the detached cells were washed with phosphate-buffered saline (PBS, Invitrogen Corp.), followed by incubation with 1% FBS in medium containing various concentrations of compound for 24 h. The wounds were photographed at 0 and 24 h on an inverted microscope (Olympus, Tokyo, Japan). The wound area was quantified using ImageJ Software (National Institutes of Health) and presented as wound healing (%) in comparison with the area of the wound at 0 h.

4.8. Cell invasion assay

Twenty-four-well transwell membrane inserts with 6.5 mm diameters and 8 μm pore sizes (Corning, Tewksbury, MA, USA) were coated with 10 μL of type I collagen (0.5 mg/mL, BD Biosciences, San Diego, CA, USA) and 20 μL of a 1:20 mixture of Matrigel (BD Biosciences)/PBS. After treatment with compounds for 24 h, MDA-MB-231 cells were harvested, resuspended in serum-free medium, and plated (0.5–1 × 10⁶ cells/chamber) in the upper chamber of the Matrigel-coated transwell insert. Medium containing 30% FBS was used as a chemoattractant in the lower chambers. At 24 h of incubation, the cells that had invaded the outer surface of the lower chambers were fixed and stained using Diff-Quik Staining Kit (Sysmex, Kobe, Japan) and imaged.⁴¹ Representative images from three separate experiments are shown, and the number of invaded cells was counted in 5 randomly selected microscopic fields (200 × magnification).

4.9. RNA isolation and real-time polymerase chain reaction (real-time PCR)

The total RNA from the cells was extracted with TRI reagent (Invitrogen, Carlsbad, CA, USA), and 1 μg of total RNA was reverse-transcribed using a Reverse Transcription System (Cat. No. A3500; Promega, Madison, WI, USA) according to the manufacturer's instructions. Real-time PCR was conducted using iQ SYBR Green Supermix (Bio-Rad, Hercules, CA, USA) according to the manufacturer's instructions. The threshold cycle (CT) was determined using Bio-Rad CFX manager 3.1 software. Relative quantification between compounds and untreated controls normalized to the levels of β-Actin mRNA was calculated using the comparative CT method.⁴² The following primers were used for real-time PCR: CDH1, 5'-GTT ATT CCT CTC CCA TCA GCT

G-3' and 5'-CTT GGC TGA GAG GAT GGT GTA A-3'; CDH2, 5'-AGC CAA CCT TAA CTG AGG AGT-3' and 5'-GGC AAG TTG ATT GGA GGG ATG-3'; ZEB1, 5'-GCA CCT GAA GAG GAC CAG AG-3' and 5'-GTG TAA CTG CAC AGG GAG CA-3'; VIM, 5'-AGA TGG CCC TTG ACA TTG AG-3' and 5'-TGG AAG AGG CAG AGA AAT CC; β-Actin, 5'-AGC ACA ATG AAG ATC AAG AT-3' and 5'-TGT AAC GCA ACT AAG TCA TA-3'.

4.10. In vivo orthotopic mouse tumor model

All animal experiments were conducted following the guidelines approved by the Seoul National University Institutional Animal Care and Use Committee (IACUC; permission number: SNU-170912–13). Female nude mice (BALB/c-nu), 5–6 weeks old, were purchased from Central Laboratory Animal, Inc. (Seoul, Korea) and housed under pathogen-free conditions with a 12 h light–dark schedule. Luciferase expressing MDA-MB-231 cells were inoculated orthotopically into the fourth fat pad of mice (1 × 10⁷ cells in 100 μL of 50:50 DMEM/Matrigel) using a 29-gauge needle. Ten days after implantation, mice were randomized into vehicle control and treatment groups of six animals per group and were administered with vehicle (EtOH/Cremophor/Normal saline = 5:5:90), **10** (5 or 15 mg/kg body weight), Psammaplin A (30 mg/kg) or Paclitaxel (5 mg/kg body weight), as a positive reference control. Compounds were administered intraperitoneally three times per week for 38 days. An additional week later, anesthetized mice were positioned in IVIS (PerkinElmer, Waltham, MA, USA) and were imaged 15 min after injection of D-luciferin (150 mg/kg, Gold Bio Technology) resuspended in PBS. Mice were Euthanized and primary tumors and organs (lungs, livers, spleens, kidneys) were excised, weighed, and frozen for further biochemical analysis or fixed for immunohistochemistry. The length (L), width (W), and height (H) of the tumors were also measured using a digital slide caliper once a week, and tumor volumes (mm³) were estimated by the formula LWH/2. Toxicity was assessed based on the lethality and body weight loss exhibited by the nude mice.⁴³

4.11. In vivo acute oral toxicity evaluation model

All animal experiments were conducted following the guidelines approved by the Seoul National University Institutional Animal Care and Use Committee (IACUC; permission number: SNU-180409–2-1). ICR mice (30 ± 2 g each) of both sexes were purchased from Central Laboratory Animal, Inc. (Seoul, Korea) and housed under pathogen-free conditions with a 12 h light–dark schedule. All the animals except control group were administered a single oral dose of compound **10** at 300 mg/kg body weight. The control animals were received only vehicle (EtOH/Cremophor/Normal saline = 5:5:90). Signs of toxicity and mortality were observed daily for 7 days.

4.12. Ex vivo immunohistochemistry and biochemical analyses of tumors

Tumor tissues fixed in 4% PFA were embedded in paraffin, sectioned mounted to slides, deparaffinized with xylene, rehydrated with ethanol series, and subjected to antigen retrieval. The slides were incubated with the indicated antibodies, which were detected using the LSAB + System-HRP kit (Dako, Glostrup, Denmark), and counterstained with hematoxylin. Stained sections were observed and imaged using a Vectra 3.0 Automated Quantitative Pathology Imaging System (Perkin Elmer, Waltham, MA, USA). A portion of frozen tumors excised from nude mice was homogenized using a hand-held homogenizer in Complete Lysis Buffer (Active Motif, Carlsbad, CA, USA) or TRI reagent (Invitrogen, Carlsbad, CA, USA). The protein expression levels of the tumor lysates were determined. The protein concentrations of tumor lysates were measured using the Bradford assay.⁴⁴

4.13. Docking methods

Molecular docking simulations were conducted using the Surflex-

Dock in Sybyl-X2.1.1 (Tripos Inc, St Louis, MO) with the crystal structures of human DOT1L (PDB: 3SR4). The 3D structures of **10** were prepared by generating 3D Concord conformations from the 2D structures. The original ligand from the X-ray structure (PDB: 3SR4) was removed and the prepared ligand **10** was docked into the crystal structure of human DOT1L. The water molecules in the active site were also removed. Staged minimization was performed with Powell's method until the gradient converged to a value of 0.5 kcal/mol·Å. Tripos force field option was applied with use current charges. Protomol was generated based on the location of the original ligand, TT8, with a threshold of 0.5 Å and bloat of 0 Å. The protein movement option was applied to allow sufficient flexibility in the binding pocket of the protein. Docking performance was validated by the docking scores along with the visual inspections of the re-docked structures compared to the original pose. Molecular interactions between the ligand and protein were further analyzed using Discovery studio 4.5 Visualizer (Biovia, San Diego, CA, USA) and PyMOL-v1.0 (Schrödinger KK, Tokyo, Japan).

Declaration of Competing Interest

The authors declare that they have no known competing financial interests or personal relationships that could have appeared to influence the work reported in this paper.

Acknowledgements

This study was supported by a grant from the National Research Foundation of Korea (NRF) funded by the Korean Government (NRF-2016M3A9B6902986).

Appendix A. Supplementary material

Supplementary data to this article can be found online at <https://doi.org/10.1016/j.bmc.2021.116072>.

References

1 Nguyen AT, Zhang Y. *Genes Dev.* 2011;25:1345–1358.

- 2 Yao Y, Chen P, Diao J, et al. *J Am Chem Soc.* 2011;133:16746–16749.
- 3 Bernt KM, Zhu N, Sinha AU, et al. *Cancer Cell.* 2011;20:66–78.
- 4 Nguyen AT, Taranova O, He J, Zhang Y. *Blood.* 2011;117:6912–6922.
- 5 Daigle SR, Olhava EJ, Therkelsen CA, et al. *Cancer Cell.* 2011;20:53–65.
- 6 Zhang L, Deng L, Chen F, et al. *Oncotarget.* 2014;5:10665–10677.
- 7 Cho MH, Park JH, Choi HJ, et al. *Nat Commun.* 2015;6:7821–7834.
- 8 Michalak EM, Visvader JE. *Mol Oncol.* 2016;10:1497–1515.
- 9 Lee JY, Kong G. *Oncotarget.* 2015;6:30451–30452.
- 10 Anglin JL, Deng L, Yao Y, et al. *J Med Chem.* 2012;55:8066–8075.
- 11 Wang Y, Li L, Zhang B, et al. *J Med Chem.* 2017;60:2026–2036.
- 12 Campbell CT, Haladyna JN, Drubin DA, et al. *Mol Cancer Ther.* 2017;16:1669–1679.
- 13 Hong S, Lee M, Jung M, Park Y, Kin M-H, Park H-g. *Tetrahedron Lett.* 2012;53:4209–4211.
- 14 Hong S, Shin Y, Jung M, et al. *Eur J Med Chem.* 2015;96:218–230.
- 15 Quinòa E, Crew CP. *Tetrahedron Lett.* 1987;28:3229–3233.
- 16 Rodriguez ADA, Akee RK, Scheuer PJ. *Tetrahedron Lett.* 1987;28:4989–4992.
- 17 Arabshahi LS, Schmitz FJ. *J Org Chem.* 1987;52:3584–3586.
- 18 Kim D, Lee IS, Jung JH, Yang SI. *Arch Pharm Res.* 1999;22:25–29.
- 19 Jung JH, Sim CJ, Lee CO. *J Nat Prod.* 1995;58:1722–1726.
- 20 Kim D, Lee IS, Jung JH, Lee CO, Choi SU. *Anticancer Res.* 1999;19:4085–4090.
- 21 Shin J, Lee H-S, Seo W, Rho J-R, Cho KW, Paul VJ. *Tetrahedron.* 2000;26:9071–9077.
- 22 Pina IC, Gautschi JT, Wang GY, et al. *J Org Chem.* 2003;68:3866–3873.
- 23 Ahn MY, Jung JH, Na YJ, Kim HS. *Gynecol Oncol.* 2008;108:27–33.
- 24 Mora FD, Jones DK, Desai PV, et al. *J Nat Prod.* 2006;69:547–552.
- 25 L.C. Clark, G.F., Jr. Combs, B.W. Turnbull, E.H. Slate, D.K. Chalker, J. Chow, L.S. Davis, R.A. Glover, G.F. Graham, E.G. Gross, A. Krongrad, J.L., Jr. Leshner, H.K. Park, B.B., Jr. Sanders, C.L. Smith and J.R. Taylor, *JAMA*, 1996;276: 1957–1963.
- 26 Moscow JA, Schmidt L, Ingram DT, Gnarra J, Johnson B, Cowan KH. *Carcinogenesis.* 1994;15:2769–2773.
- 27 Calvo A, Xiao N, Kang J, et al. *Cancer Res.* 2002;62:5325–5335.
- 28 Hu YJ, Diamond AM. *Cancer Res.* 2003;63:3347–3351.
- 29 Meplan C, Nicol F, Burtle BT, et al. *Antioxid Redox Signal.* 2009;11:2631–2640.
- 30 Sanmartin C, Plano D, Palop JA. *Mini Rev Med Chem.* 2008;8:1020–1031.
- 31 Sahu PK, Umme T, Yu J, et al. *J Med Chem.* 2015;58:8734.
- 32 Sahu PK, Kim G, Nayak A, et al. *Asian J Org Chem.* 2016;5:183–186.
- 33 Yu J, Zhao LX, Park J, et al. *J Med Chem.* 2017;60:3422–3437.
- 34 Yu J, Ahn S, Kim HJ, et al. *J Med Chem.* 2017;60:7459–7475.
- 35 Byun WS, Kim WK, Han HJ, et al. *Mol Ther Oncolytics.* 2019;15:140–152.
- 36 Byun WS, Kim WK, Yoon JS, Jarhad DB, Jeong LS, Lee SK. *Biomolecules.* 2020;10:530–545.
- 37 Anglin JN, Song Y. *J Med Chem.* 2013;56:8972–8983.
- 38 Vichai V, Kirtikara K. *Nat Protoc.* 2006;1:1112–1116.
- 39 Smith PK, Krohn RI, Hermanson GT, et al. *Anal Biochem.* 1985;150:76–85.
- 40 Kim WK, Byun WS, Chung HJ, et al. *Biochem Pharmacol.* 2018;152:71–83.
- 41 Park SK, Byun WS, Lee S, et al. *Biochem Pharmacol.* 2020;178:114053–114067.
- 42 Byun WS, Jin M, Yu J, et al. *Biochem Pharmacol.* 2018;158:84–94.
- 43 Byun WS, Kim S, Shin YH, Kim WK, Oh D-C, Lee SK. *J Nat Prod.* 2020;83:118–126.
- 44 Bradford MM. *Anal Biochem.* 1976;72:248–254.